12^{th} International Conference on Fracture Mechanics of Concrete and Concrete Structures
FraMCoS-12
B.L.A. Pichler, Ch. Hellmich, P. Preinstorfer (Eds)

https://doi.org/10.21012/FC12.1226
MS02-3:4

ON THE CORRELATION BETWEEN THE STABLE RATE OF DEFORMATION GROWTH AND THE FATIGUE LIFE IN CONCRETE

Wassim Kerkeni[1], Abedulgader Baktheer[1], Mario Aguilar[1], Henrik Becks[1], Martin Classen[1], Rostislav Chudoba[1]

[1] Institute of Structural Concrete, RWTH Aachen University,
Mies-van-der-Rohe-Str. 1, 52074 Aachen, Germany, abaktheer@imb.rwth-aachen.de

Key words: Fatigue, Concrete, Loading rate effect, S-N curves, Experimental investigations

Abstract. For the reliable and economical design of concrete structures under fatigue loading, a comprehensive understanding and accurate prediction of concrete fatigue life, especially under complex loading scenarios with variable amplitudes, is critical. Recent experimental studies on concrete compressive fatigue behavior demonstrate that fatigue life is closely linked to the strain rate in the second phase of strain development. Based on extensive testing of cylindrical specimens, a linear relationship between the strain rate in this phase and the number of cycles to failure has been observed in double-logarithmic space. This correlation provides a more consistent evaluation of fatigue life with significantly less scatter compared to traditional S-N curves. Moreover, the predictive capability of the strain-rate criterion can be used to estimate the fatigue life of runouts, which also enables the possibiliy of highly accelerated fatigue tests.

This contribution extends the analysis of the linear correlation across a broader range of fatigue stress configurations and varied parameters. In addition to compressive fatigue behavior observed through cylindrical tests, experimental data on tensile fatigue, using notched three-point bending tests (3PBT), and shear fatigue, using punch-through shear tests (PTST), are evaluated. Furthermore, this study re-evaluates the effect of loading sequence—a key factor in fatigue design—by applying the strain rate criterion across different stress states.

1 INTRODUCTION

Realistic modeling of concrete fatigue behavior is essential to ensure structural safety and sustainability. Particularly, bridges and wind turbine towers are exposed to high-cycle loading due to their slender cross sections, leading to a significant increase in demand for new constructions in the coming decades [1, 2, 3, 4]. Currently, researchers are exploring various monitoring concepts for the strain development of concrete structures under fatigue loading [5, 6, 7]. Combined with a suitable method to evaluate the fatigue life, the developed measurement concepts could be used to reliably predict the remaining service life of existing structures. The fatigue life of concrete is typically characterized by the Wöhler / S-N diagrams [8, 9, 10, 11]. However, as a strength-based criterion, S-N diagrams do not represent the degradation process during the fatigue life. Therefore, no connection can be established with the new monitoring concepts. Within experimental investigations, the Wöhler curves also show a considerable scatter, which complicates a reliable assessment of fatigue life. The fatigue degradation process is typically captured by plotting the increasing strain as a function of the number of load cycles applied at the subcritical level. This function, qualitatively depicted in Fig. 1a and referred to as fatigue

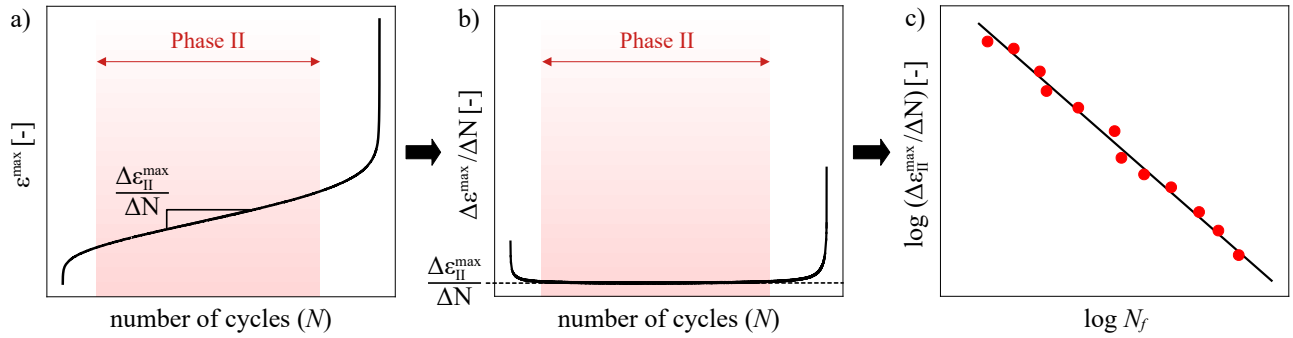

Figure 1: a) Typical fatigue creep curve characterized by linear growth in the second phase b) Relationship between strain rate and number of cycles to failure, displaying a constant secondary strain rate c) Simplified illustration of the Sparks-Menzies relation

creep curve in the sequel, comprises three distinct phases: an initial rapid increase up to 20% of the lifetime, followed by a linear increase up to 80% of consumed life, and finally an accelerated growth leading to failure. Sparks and Menzies [12] noted a linear relationship between the number of cycles to failure N_f and the slope of the strain growth during the second phase of the fatigue creep curve, i.e. the secondary strain rate $\Delta\varepsilon_{\mathrm{II}}^{\max}/\Delta N$, in double logarithmic space. This relationship is illustrated in Fig. 1c and defined by

$$\log \frac{\Delta\varepsilon_{\mathrm{II}}^{\max}}{\Delta N} = m + s \log N_f. \qquad (1)$$

The linear correlation provides a strain-based approach to precisely evaluate fatigue life and could thus be integrated into monitoring concepts.

In recent years, the validity of the Sparks-Menzies relation has been assessed in experimental studies focused mainly on the compressive fatigue behavior of concrete. The relationship was found to be independent of fibre content [13], specimen size [14] and loading frequency [15], suggesting that it solely depends on the concrete matrix. However, in order to draw definitive conclusions, further investigations are required considering a broader range of test setups and load configurations.

The present evaluation draws on several experimental studies previously published by the authors. In order to facilitate the examination of compressive, tensile and shear fatigue behavior, the Sparks-Menzies relation is applied to cylinder tests, three-point bending tests and punch-through shear tests. For each experimental series, the evaluation of fatigue life is conducted based on both the Wöhler curves and the Sparks-Menzies relation, enabling a qualitative comparison of the evaluation methods across a broad range of load configurations and varied parameters. Fig. 2 provides an overview of the comprehensive experimental program, alongside the structure of the paper. The particular test configurations and experimental results are presented and discussed in each subsection.

2 CYLINDER TEST

2.1 Varied loading frequencies

Test configuration: The experimental series with varied loading frequencies is part of the study presented in [16]. According to fib Model Code 2010 [17] the concrete used in this test series can be classified into concrete strength class C40. The fatigue tests have been performed using cylinder specimens with a diameter of 150 mm and a height of 300 mm. Throughout the experiments, the strains of the concrete cylinders were measured continuously using linear variable differential transformers (LVDTs). Three LVDTs were attached around the specimen, each with a 120-degree offset. The loading scenario is based on standard fatigue loading with constant amplitudes. The load was applied with frequencies of 2 Hz, 8.5 Hz and 55 Hz. The upper load levels varied between $S_{\max}$ = 0.65 and $S_{\max}$ = 0.80, while the lower load level was set to $S_{\min}$ = 0.05.

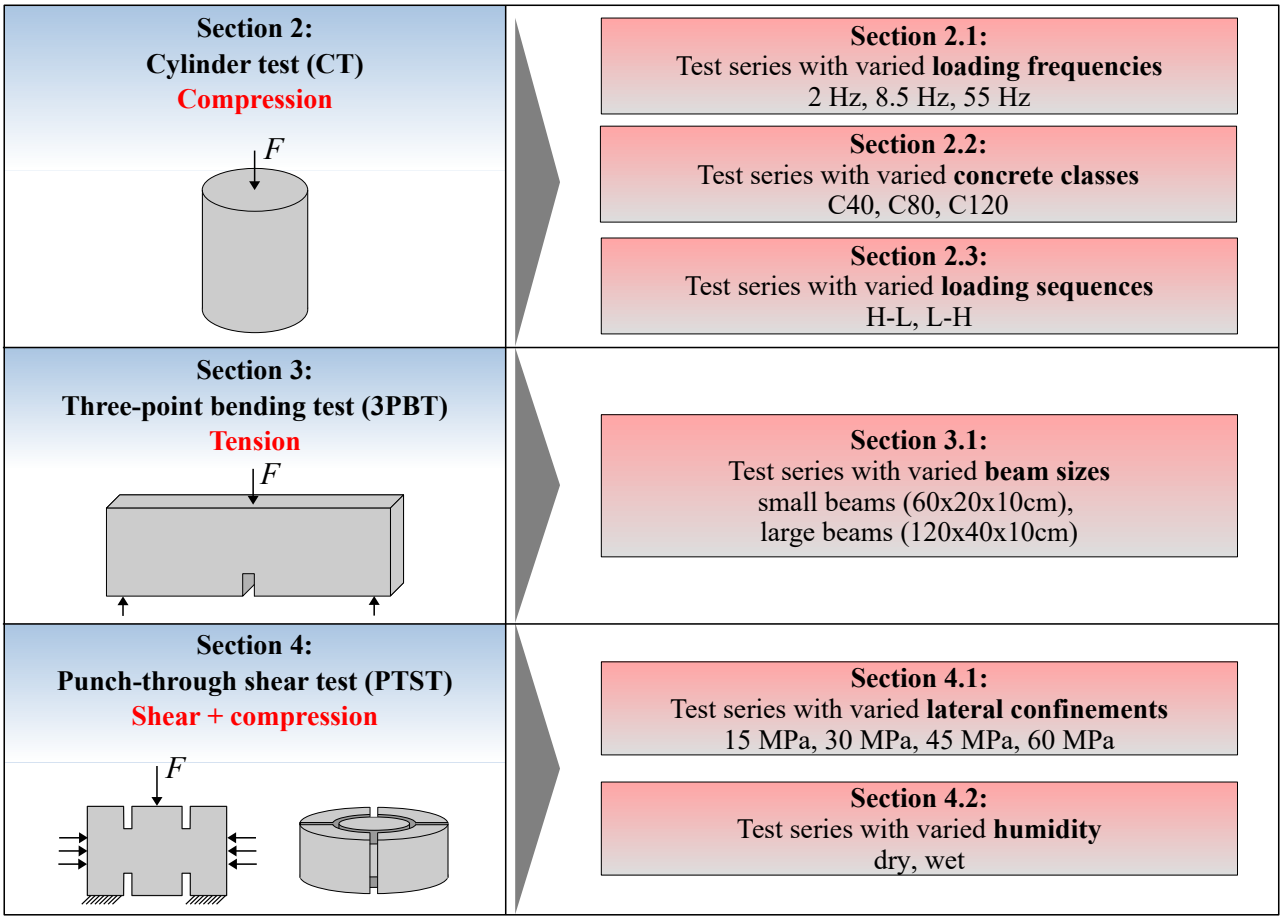

Figure 2: Overview of the test setups and evaluated test series with varied parameters, alongside the structure of the paper

Wöhler curves: The number of cycles to failure for varied upper load levels $S_{\max}$ measured in the fatigue tests at f = 2 Hz, f = 8.5 Hz and f = 55 Hz is summarized in Fig 3a. The fib Model Code 2010 [17] proposes an empirical approximation of Wöhler curves for the normal- and high strength concrete by defining the number of cycles to failure in the range $\log\, N \leq 8$ as

$$\log\, N_f = \frac{8}{Y-1}\,(S_{\max}-1) \tag{2}$$

where

$$Y = \frac{0,45 + 1,8\; S_{\min}}{1 + 1,8\; S_{\min} - 0,3\;(S_{\min})^2}. \tag{3}$$

For all investigated loading frequencies, the established regression lines do not match well with the Wöhler curves evaluated using the approximation Eq. (2). In order to reliably assess fatigue life using the Wöhler curves, more tests would be necessary.

Sparks-Menzies relation: For each test, the secondary strain rate was determined and then plotted on a double logarithmic scale with respect to the number of cycles to failure, as depicted in Fig. 3b. Regarding the coefficients of determination (R^2) in Table 1, strong linear correlations can be observed for the fatigue tests conducted with loading frequencies of f = 2 Hz and f = 8.5 Hz. Due to the very high frequency and the small number of evaluated tests, no equivalent result could be obtained for f = 55 Hz. With high loading frequencies, factors such as heat generation can play a significant role in determining fatigue life, which complicates an accurate evaluation based on the strain-rate criterion. Nevertheless, the depiction of individual regression lines for each loading frequency allows the observation of trends, which cannot be displayed in an S-N diagram. By comparing the regression lines,

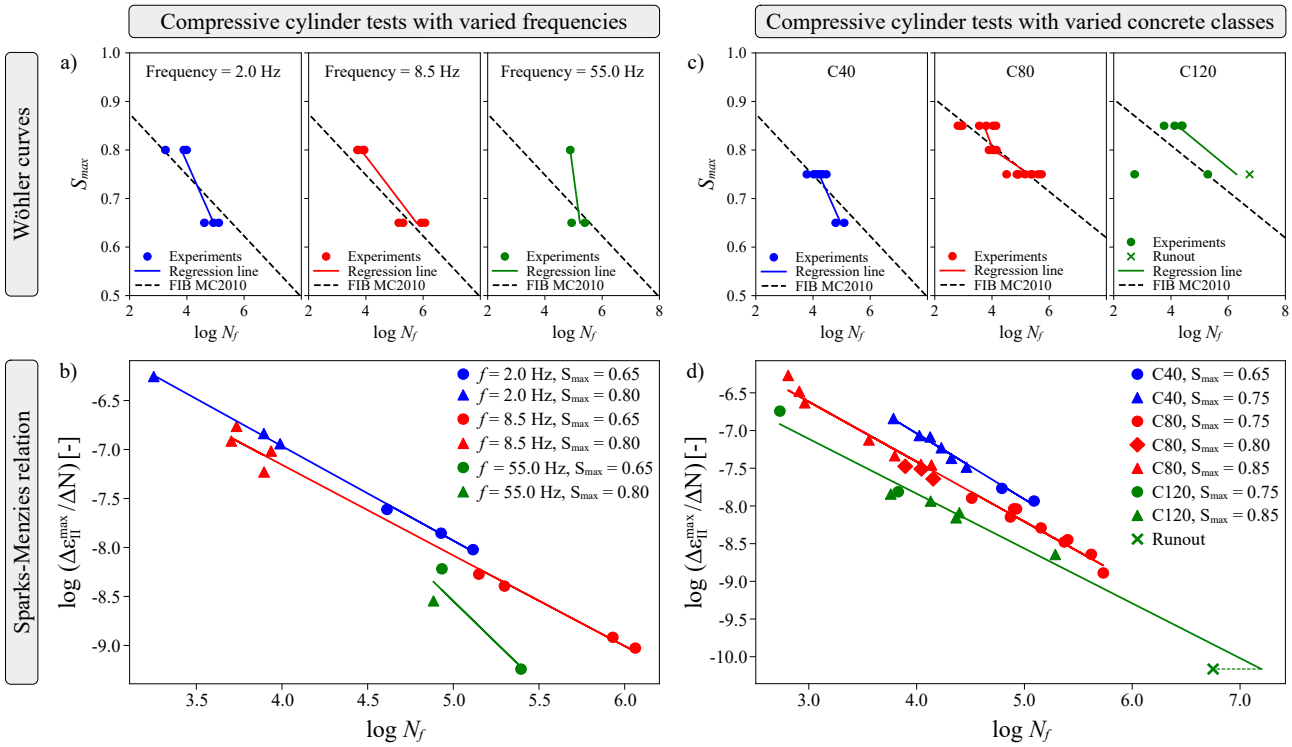

Figure 3: Evaluation of compressive fatigue life using cylinder tests with varied loading frequencies and concrete classes: a) Wöhler curves for the tests with loading frequencies of 2 Hz, 8.5 Hz and 55 Hz; b) Sparks-Menzies relation shown with regression lines for each loading frequency; c) Wöhler curves for concrete C40, C80 and C120 d) Sparks-Menzies relation shown with regression lines for each concrete class

we can observe that an increase in loading frequency leads to a decrease in secondary strain rates. However, if a higher number of tests had been conducted, it could be argued that the data points for f = 2 Hz and f = 8.5 Hz could follow the same linear alignment, as only a slight scatter is observed despite the varying loading frequencies.

2.2 Varied concrete classes

Test configuration: The experimental series with varied concrete classes is part of the study presented in [18]. The cylinder test specimens can be classified into strength classes C40, C80 and C120. Each specimen measured between 100-150 mm in diameter and 300 mm in height. As in the previous test series (Sec. 2.1), three LVDTs were used to monitor the strain development throughout the experiments. In the constant-amplitude fatigue tests, the load was applied with a frequency of 5 Hz. The upper load levels ranged from $S_{\max}$ = 0.65 to $S_{\max}$ = 0.85, while lower load levels remained constant at $S_{\min}$ = 0.05 and $S_{\min}$ = 0.20.

Wöhler curves: The Wöhler curves for the fatigue tests conducted with concrete C40, C80 and C120 are plotted in Fig. 3c. Among the investigated concrete classes, the regression line for C80 exhibits the best alignment with the approximated Wöhler curve based on Eq. (2). It is particularly evident that the obtained results for concrete class C120 show a pronounced scatter, causing the regression line to display a longer fatigue life than predicted by the fib Model Code 2010. More tests would have been required to establish reliable Wöhler curves for concrete C40 and C120.

Sparks-Menzies relation: Fig. 3d shows the logarithmic secondary strain rate versus the logarithmic number of cycles to failure for each test. It can be observed that the data points for each concrete class align very well with their

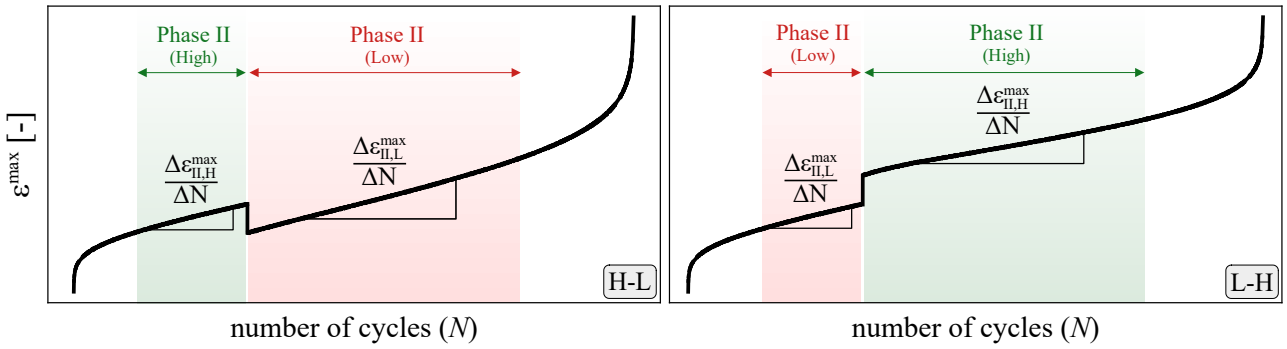

Figure 4: Determination of the secondary strain rates $\Delta\varepsilon^{\max}_{\mathrm{II,H}}/\Delta N$ and $\Delta\varepsilon^{\max}_{\mathrm{II,L}}/\Delta N$ in (H-L) and (L-H) loading scenarios

respective regression lines. Moreover, there is a clear trend showing that higher compressive strength results in lower secondary strain rates. As the compressive strength increases, concrete exhibits less plastic deformation, leading to a slower strain rise in the second fatigue phase.

The experimental series on the C120 concrete included a runout specimen, as one test had to be stopped after around 5.6 million loading cycles without fatigue failure. The importance of the Sparks-Menzies relation is particularly demonstrated by the analysis of such runouts. Although the specimen did not fail, we can use the obtained regression line to reliably predict the actual failure point. The secondary strain rate was therefore determined based on the monitored strain history in order to plot the runout as a data point in the diagram, as shown in Fig. 3d. Based on the extrapolated regression line, the number of cycles to failure for this test is predicted to be approximately 15.8 million.

2.3 Varied loading sequences

Test configuration: The C40 cylinders from the previous experimental series were also used in further fatigue tests with varied loading sequences [18]. The fatigue loading was applied with a frequency of 5 Hz at two distinct levels in different sequences: high-low (H-L) and low-high (L-H). The upper load level $S_{\max}$ was set to 0.75 and 0.65 for the higher loading range (H) and the lower loading range (L), respectively. Throughout all conducted experiments $S_{\min}$ remained constant at 0.05. In the loading scenarios (H-L) and (L-H) the first load level was applied with a specified number of cycles, then the second load level was applied until fatigue failure.

Experimental results: This section discusses a new approach to analyze the sequence effect in the compressive fatigue behavior of concrete based on the Sparks-Menzies relation. Fig. 4 illustrates simplified fatigue creep curves for the (H-L) and (L-H) scenarios. It can be observed that the strain rate $\Delta\varepsilon^{\max}_{\mathrm{II,H}}/\Delta N$ is determined within the second phase of the higher load range (H) and the strain rate $\Delta\varepsilon^{\max}_{\mathrm{II,L}}/\Delta N$ within the second phase of the lower load range (L). These strain rates can be used to obtain the theoretical numbers of cycles to failure N^t_H and N^t_L at constant amplitudes. Initially, a Sparks-Menzies equation Eq. (1) must be defined, based on a constant-amplitude experimental campaign conducted on identical concrete. The theoretical number of cycles to failure N^t_H is then calculated by rearranging Eq. (1) into

$$N^t_H = 10^{\dfrac{\log\left(\frac{\Delta\varepsilon^{\max}_{\mathrm{II,H}}}{\Delta N}\right) - m}{s}} \tag{4}$$

while N^t_L is determined by an analogous equation. The concrete used in the test series with varied loading sequences is classified into concrete strength class C40. In Sec. 2.2, a regression line for constant-amplitude fatigue tests conducted with C40 concrete cylinders has already been established using the Sparks-Menzies relation (Fig. 3d). For each (H-L) and

(L-H) test, N_H^t and N_L^t can therefore be obtained based on the regression line and the previously described determination of $\Delta\varepsilon_{\mathrm{II,H}}^{\max}/\Delta N$ and $\Delta\varepsilon_{\mathrm{II,L}}^{\max}/\Delta N$. Within this experimental evaluation, the consumed fatigue life η is calculated from the quotient of the applied load cycle number and the theoretical number of cycles to failure. The consumed fatigue life during (H) scenario η_H is therefore given by:

$$\eta_H = \frac{N_H}{N_H^t} \tag{5}$$

For the load level (L), an analogous calculation is performed to obtain η_L. In a given experiment, the total fatigue life $\sum\eta$ is ultimately calculated as the sum of η_H and η_L. Based on the Palmgren-Miner rule, $\sum\eta$ should always be equal to 1, as the widely adopted rule assumes that the overall fatigue life can be predicted by a linear interpolation of the fatigue life for each load range separately.

The results of all evaluated cylinder tests with (H-L) and (L-H) loading scenarios are compared with the prediction of the Palmgren-Miner rule and plotted in terms of consumed fatigue life diagrams in Fig. 5. The tests were evaluated based on both the strain-rate criterion (Fig. 5a) and the Wöhler curves (Fig. 5b), enabling a direct comparison between the evaluation methods. In the diagrams, the horizontal axis represents the determined values η_H for the (H-L) tests and η_L for the (L-H) tests, while the vertical axis represents the sum of the consumed fatigue life. Regarding the strain-based evaluation of the (H-L) tests, the average of the consumed fatigue life sum $\sum\eta$ equals 0.79. This indicates an unsafe prediction of the P-M rule for the (H-L) scenario. The evaluation based on the Wöhler curves indicates an identical trend for the experiments considered here. The mean value of the sum of the fatigue lifetimes was also calculated to be 0.79. In terms of the (L-H) scenario, applying the strain-rate criterion resulted in an average of the consumed fatigue life sum of 0.69. Consequently, the P-M rule provides an unsafe predicition for the (L-H) scenario as well. A significant difference is evident when compared to the obtained results based on the Wöhler curves, where the mean value of $\sum\eta$ was determined to be 1.07. This indicates a conservative prediction of the P-M rule for the (L-H) scenario, a finding that is further substantiated by various studies [19, 20, 21]. By comparing the diagrams in Fig. 5, it becomes apparent that the strain-rate criterion enabled an evaluation with significantly less scatter compared to the evaluation based on the Wöhler curves.

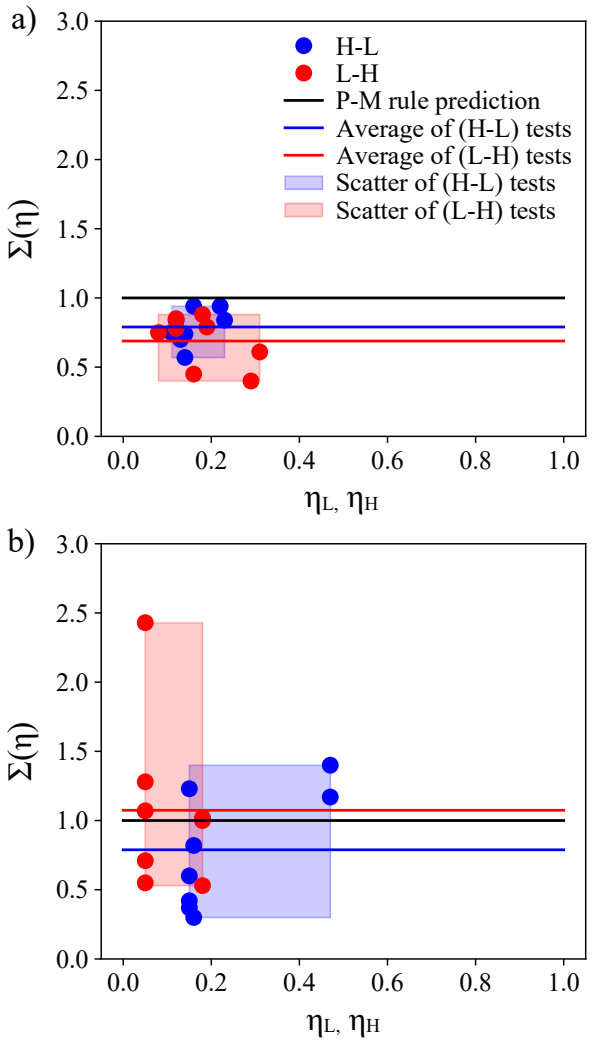

Figure 5: Results of the tests with (H-L) and (L-H) loading scenarios summarized in consumed fatigue life diagrams: a) Evaluation based on the strain-rate criterion; b) Evaluation based on the Wöhler curves

However, more tests need to be evaluated in order to definitively validate the observed trends. Within this study, only eight tests each for the

(H-L) and (L-H) scenario could be considered from the original test series [18], as several tests did not contain clear linear branches within their fatigue creep curves, making it impossible to determine the secondary strain rates.

3 THREE-POINT BENDING TEST

3.1 Varied specimen size

Test configuration: The three-point bending tests with varied beam sizes are part of the study presented in [22]. The concrete used in the tensile fatigue tests can be classified into concrete strength class C60. The notched beam specimens were produced in two different sizes. The cross-sectional height of the larger beams was h = 400 mm, while the height of the smaller beams was h = 200 mm. The beam width remained constant at b = 100 mm. To continuously monitor the crack tip opening displacement (CTOD) throughout the experiments, two LVDTs were attached at the top of the notch in both sides of the beam. Additionally, a third LVDT measured the mid-span deflection. The constant-amplitude fatigue loading was applied with a frequency of 5 Hz. The upper load levels varied between $S_{\max}$ = 0.70 and $S_{\max}$ = 0.85, while the lower load level was set to $S_{\min}$ = 0.05.

Wöhler curves: The established Wöhler curves for both beam sizes are shown in Fig. 6a. Despite the limited number of evaluated tests, the regression line for the small beams matches well with the Wöhler curve based on the approximation in Eq. (2). However, the test results obtained for the large beams show a considerable scatter, particularly at the load level $S_{\max}$ = 0.70. Thus, no reliable Wöhler curve could be established for the large beams.

Sparks-Menzies relation: The slope within the second phase of the measured CTOD development was determined for each test and subsequently plotted on a double logarithmic scale against the number of cycles to failure, as depicted in Fig. 6b.

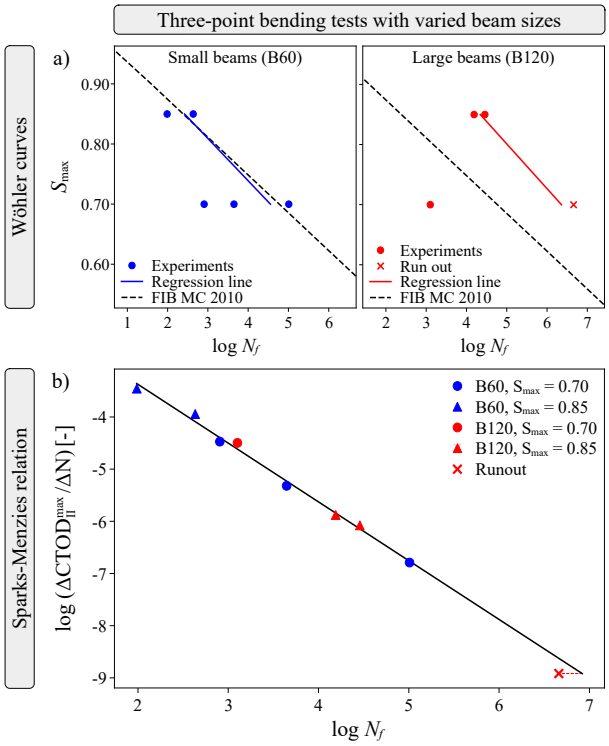

Figure 6: Evaluation of tensile fatigue life using three-point bending tests: a) Wöhler curves for small and large beams; b) Sparks-Menzies relation shown with a combined regression line for small and large beams

It can be observed that all the data points align very well with a single regression line, independent of the specimen size. The obtained result provides further evidence that the Sparks-Menzies relation is size-independent, as previously observed by Ortega et al. [14]. Within the experimental series on the large beams, one test had to be stopped since no fatigue failure occurred after around 4.5 million loading cycles. As already demonstrated in Sec. 2.2, the Sparks-Menzies relation can be used to estimate the fatigue life of runout specimens. In this instance, the slope within the second phase of the monitored CTOD development was determined to then predict a number of cycles to failure of approximately 8.3 million.

4 PUNCH-THROUGH SHEAR TEST

4.1 Varied lateral confinement

Test configuration: The punch-through shear tests (PTSTs) with varied lateral confinements are part of the studies presented in [23]. A high-

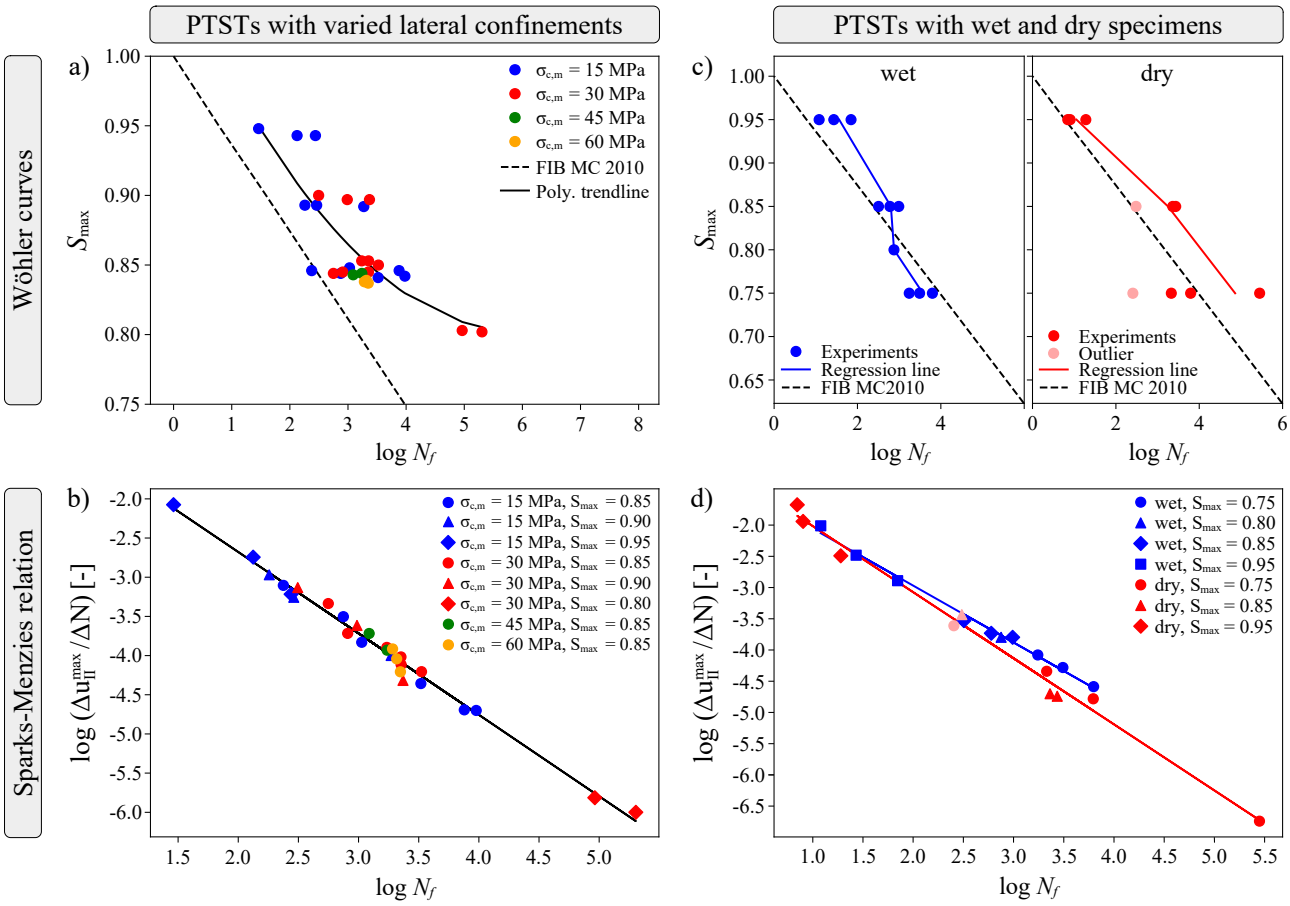

Figure 7: Evaluation of multi-axial fatigue life using punch-through shear tests: a) Wöhler curves for the tests with varied lateral confinements; b) Sparks-Menzies relation shown with a combined regression line for the tests with varied lateral confinements; c) Wöhler curves for the tests with wet and dry specimens d) Sparks-Menzies relation shown with regression lines for the wet and dry tests

strength concrete (f_c = 96 MPa) was used in the multi-axial fatigue tests. In the bottom-left corner of Fig. 2, a simplified illustration of the notched test specimen is shown. Throughout the experiments, the displacement of the crack surfaces was measured continuously using six LVDTs, which were attached to the bottom and top of the specimen. The fatigue tests were conducted with constant amplitudes and a loading frequency of 5 Hz. The upper load levels varied between $S_{\max}$ = 0.80 to $S_{\max}$ = 0.95, while the lower load level was set to $S_{\min}$ = 0.05. The applied lateral compressive stress $\sigma_{c,\text{mean}}$ ranged from 15 to 60 MPa.

Wöhler curve: In Fig. 7a, the applied upper load levels $S_{\max}$ are plotted with respect to the logarithmic number of cycles to failure measured in fatigue tests with different lateral compressive stresses $\sigma_{c,\text{mean}}$. The illustrated polynomial trendline displays a longer fatigue life than predicted by the fib Model Code 2010. Since the results for all levels of $\sigma_{c,\text{mean}}$ are combined into a single diagram, a substantial scatter is observed, complicating the reliable assessment of fatigue life based on the S-N diagram. However, the findings suggest that fatigue life appears to be independent of σ_c, with the scatter decreasing significantly as σ_c increases.

Sparks-Menzies relation: The logarithmic secondary displacement rate versus the logarithmic number of cycles to failure is plotted in Fig. 7b for each test. Despite the varying testing configurations, all data points follow the same linear alignment. Thus, it can be concluded that

	CTs with varied loading frequencies and concrete classes						3PBTs with varied beam sizes	PTSTs with varied lateral confinements	PTSTs with varied humidity	
	2.0 Hz	**8.5 Hz**	**55.0 Hz**	**C40**	**C80**	**C120**	**B60 & B120**	**15 - 60 MPa**	**wet**	**dry**
m	-3.106	-3.454	-0.023	-3.546	-4.234	-4.929	-1.121	-0.600	-1.147	-0.957
s	-0.965	-0.925	-1.705	-0.873	-0.795	-0.727	-1.127	-1.039	-0.911	-1.058
R²	0.998	0.989	0.844	0.987	0.985	0.954	0.993	0.989	0.993	0.990

Table 1: Overview of regression constants m and s based on Eq. (1), with the coefficient of determination (R^2) values for each experimental series

the Sparks-Menzies relation is also independent of σ_c.

4.2 Varied humidity

Test configuration: In a subsequent experimental campaign, PTSTs were conducted to examine the influence of material moisture. The concrete utilized was identical to that employed in the previous study [23], but the specimens were stored in a water bath for two months immediately after demolding. Two moisture conditions were distinguished: wet (stored in the water bath until testing) and dry (dried at 105°C for one month prior to testing). The constant-amplitude fatigue loading was applied with a frequency of 2 Hz. The upper load levels ranged from $S_{\max}$ = 0.75 to $S_{\max}$ = 0.95, while the lower load level remained constant at $S_{\min}$ = 0.05. The lateral compressive loading was set to $\sigma_{c,\text{mean}}$ = 20 MPa.

Wöhler curves: The established Wöhler curves of the fatigue tests conducted with wet and dry specimens are shown in Fig. 7c. Within the S-N diagram for the dry specimens, it can be observed that two tests are shown as outliers. These tests exhibited a pronounced angular misalignment of the testing surface resulting in an asymmetrical load distribution, which led to a significant reduction of fatigue life based on an unintentional stress concentration on one side of the fracture surface.

Sparks-Menzies relation: For each test, the secondary displacement rate was determined and then plotted on a double logarithmic scale with respect to the number of cycles to failure, as depicted in Fig. 7d. Within this experimental evaluation, the fatigue tests conducted with wet and dry specimens cannot be represented based on a single regression line. Thus, the independence between the Sparks-Menzies relation and the moisture content in concrete is not definitively proven. However, it can be observed that the data points for each humidity level align very well with their respective regression lines. Notably – despite the asymmetrical load distribution – both tests identified as outliers align closely with the linear trend observed for all dry fatigue tests. Thus, while the reduced fatigue life caused by the unintentionally generated stress concentration may result in pronounced scatter within the stress-based Wöhler diagram, this experimental error does not affect the evaluation based on the Sparks-Menzies relation, as the reduced fatigue life simultaneously results in higher displacement rates within the second fatigue phase.

5 CONCLUSIONS

Based on the evaluation of the comprehensive experimental data presented in this paper, the following conclusions and suggestions for future research can be made:

- The presented strain-rate criterion can be applied to precisely evaluate the fatigue life under compressive, tensile and shear loading. It offers a more reliable assessment of fatigue life with significantly reduced scatter compared to conventional Wöhler curves, making it an excellent approach for predicting a structure's remaining service life. More-

over, the strain-based evaluation method can be used to estimate the failure point of runout specimens.

- The Sparks-Menzies relation was applied in compressive cylinder test series with varied loading frequencies and concrete classes. Besides the reliable evaluation of fatigue life, the strain-rate criterion allowed the observation of trends, which cannot be displayed in an S-N diagram: The secondary strain rate decreases with both increasing loading frequency and concrete class.

- This study presented a new approach to analyze the sequence effect in the compressive fatigue behavior of concrete by applying the strain-rate criterion across different load levels. In relation to the P-M rule, the experimental evaluation indicated that both the (H-L) and (L-H) scenarios lead to a fatigue life reduction. However, the difficult identification of linear branches within the fatigue creep curves of the (H-L) and (L-H) tests complicated a strain-based interpretation of the sequence effect. Thus, adjustments of the presented evaluation methodology are essential to ensure reliable results.

- The evaluation of the three-point bending tests showed that the Sparks-Menzies relation is size-independent. Regardless of the beam size, all data points aligned very well with a single regression line.

- The evaluation of the punch-through shear tests showed that the Sparks-Menzies relation is also independent of the lateral compressive stress. However, the independence of moisture content was not definitively proven.

- The established correlation between strain rate and fatigue life demonstrates significant potential as a criterion for integration into advanced modeling approaches, such as those presented in [24, 25, 26]. This integration could facilitate the development of more efficient and reliable fatigue simulation tools, contributing to improved performance assessments and the design of concrete structures subjected to fatigue loading.

All presented regression lines obtained from the Sparks-Menzies relation are defined in Table 1, where the regression constants m and s based on Eq. (1), alongside the coefficients of determination R^2 are shown for every test series.

REFERENCES

[1] A. Baktheer, C. Goralski, J. Hegger, R. Chudoba, Stress configuration-based classification of current research on fatigue of reinforced and prestressed concrete, Structural Concrete (2024). doi:10.1002/suco.202300667.

[2] A. Baktheer, S. Esfandiari, M. Aguilar, H. Becks, M. Classen, R. Chudoba, Fatigue-induced stress redistribution in prestressed concrete beams modeled using the constitutive hypothesis of inter-aggregate degradation, Fatigue & Fracture of Engineering Materials & Structures (2024). doi:10.1111/ffe.14388.

[3] M. Aguilar, A. Baktheer, R. Chudoba, Multi-axial fatigue of high-strength concrete: Model-enabled interpretation of punch-through shear test response, Engineering Fracture Mechanics 311 (2024) 110532. doi:10.1016/j.engfracmech.2024.110532.

[4] H. Becks, M. Aguilar, A. Baktheer, R. Chudoba, M. Classen, Experimental and numerical investigations on the fatigue behavior of high-strength concrete under combined shear-compression loading, in: IABSE Proceedings of IABSE symposium: challenges for existing and oncoming structures, Prague, Czech Republic, 2022, p. 532–540.

[5] H. Becks, A. Baktheer, S. Marx, M. Classen, J. Hegger, R. Chudoba, Monitoring concept for the propagation of compressive fatigue in externally prestressed concrete beams using digital

image correlation and fiber optic sensors, Fatigue & Fracture of Engineering Materials & Structures 46 (2) (2023) 514–526. doi:10.1111/ffe.13881.

[6] F. Seemab, M. Schmidt, A. Baktheer, M. Classen, R. Chudoba, Automated detection of propagating cracks in rc beams without shear reinforcement based on dic-controlled modeling of damage localization, Engineering Structures 286 (2023) 116118. doi:10.1016/j.engstruct.2023.116118.

[7] H. Becks, L. Lippold, P. Winkler, M. Moeller, M. Rohrer, T. Leusmann, D. Anton, B. Sprenger, P. Kähler, I. Rudenko, D. Andrés Arcones, P.-S. Koutsourelakis, J. F. Unger, M. Weiser, Y. Petryna, M. Schnellenbach-Held, D. Lowke, H. Wessels, A. Lenzen, V. Zabel, C. Könke, M. Claßen, J. Hegger, Neuartige Konzepte für die Zustandsüberwachung und -analyse von Brückenbauwerken – Einblicke in das Forschungsvorhaben SPP100+, Bauingenieur 99 (10) (2024) 327–338. doi:10.37544/0005-6650-2024-10-63.

[8] S. Schneider, Frequenzabhängigkeit des ermüdungswiderstandes von hochfestem beton (2021).

[9] C. Tomann, N. Oneschkow, Influence of moisture content in the microstructure on the fatigue deterioration of high-strength concrete, Structural Concrete 20 (4) (2019) 1204–1211. doi:10.1002/suco.201900023.

[10] A. Baktheer, H. Spartali, R. Chudoba, J. Hegger, Concrete splitting and tip-bearing effect in the bond of anchored bars tested under fatigue loading in the push-in mode: An experimental investigation, Materials and Structures 55 (3) (2022) 101. doi:10.1617/s11527-022-01935-7.

[11] A. Baktheer, B. Camps, J. Hegger, R. Chudoba, Numerical and experimental investigations of concrete fatigue behaviour exposed to varying loading ranges, in: fib congress. Melbourne, 2018, no. ISBN: 978-1-877040-15-3, 2018, pp. 1110–1123.

[12] P. R. Sparks, J. B. Menzies, The effect of rate of loading upon the static and fatigue strengths of plain concrete in compression, Magazine of Concrete Research (83) (1973).

[13] E. Poveda, G. Ruiz, H. Cifuentes, R. C. Yu, X. Zhang, Influence of the fiber content on the compressive low-cycle fatigue behavior of self-compacting sfrc, International Journal of Fatigue 101 (2017) 9–17. doi:10.1016/j.ijfatigue.2017.04.005.

[14] J. J. Ortega, G. Ruiz, E. Poveda, D. C. González, M. Tarifa, X. X. Zhang, R. C. Yu, M. Vicente, Á. de La Rosa, L. Garijo, Size effect on the compressive fatigue of fibre-reinforced concrete, Construction and Building Materials 322 (2022) 126238. doi:10.1016/j.conbuildmat.2021.126238.

[15] C. von der Haar, J. Hümme, S. Marx, L. Lohaus, Untersuchungen zum ermüdungsverhalten eines höherfesten normalbetons, Beton- und Stahlbetonbau 110 (10) (2015) 699–709. doi:10.1002/best.201500034.

[16] A. Baktheer, R. Chudoba, Experimental study of the interacting effects of loading rate and temperature on concrete fatigue behavior under compression, Construction and Building Materials (2024). doi:10.1016/j.conbuildmat.2024.139466.

[17] F. model code, Fib model code for concrete structures 2010, Document Competence Center Siegmar Kästl eK, Germany.

[18] A. Baktheer, R. Chudoba, Experimental and theoretical evidence for the load sequence effect in the compressive fatigue behavior of concrete, Materials and Structures 54 (2) (2021) 82. doi:10.1617/s11527-021-01667-0.

[19] J. O. Holmen, Fatigue of concrete by constant and variable amplitude loading, ACI Journal, Special Publication 75 (1982) 71–110. doi:10.14359/6402.

[20] G. Petkovic, R. Lenschow, H. Stemland, S. Rosseland, Fatigue of high-strength concrete, Special Publication 121 (1990) 505–526. doi:10.14359/3740.

[21] M. Aguilar, A. Baktheer, R. Chudoba, Numerical investigation of load sequence effect and energy dissipation in concrete due to compressive fatigue loading using the new microplane fatigue model MS1, Onate, E., Peric, D., Chiumenti, M., de Souza Neto, E., Eds; COMPLAS 2021; Barcelona, Spain, 2021. doi:10.23967/complas.2021.053.

[22] A. Baktheer, H. Becks, Fracture mechanics based interpretation of the load sequence effect in the flexural fatigue behavior of concrete using digital image correlation, Construction and Building Materials 307 (2021). doi:10.1016/j.conbuildmat.2021.124817.

[23] H. Becks, M. Aguilar, R. Chudoba, M. Classen, Characterization of high-strength concrete under monotonic and fatigue mode II loading with actively controlled level of lateral compression, Materials and Structures 55 (10) (2022) 252. doi:10.1617/s11527-022-02087-4.

[24] A. Baktheer, M. Aguilar, R. Chudoba, Microplane fatigue model MS1 for plain concrete under compression with damage evolution driven by cumulative inelastic shear strain, International Journal of Plasticity 143 (2021). doi:10.1016/j.ijplas.2021.102950.

[25] M. Aguilar, A. Baktheer, H. Becks, M. Classen, R. Chudoba, Fatigue-induced concrete fracture under combined compression and shear studied using standard cylinder and refined punch-through shear test setup, 11th International Conference on Fracture Mechanics of Concrete and Concrete Structures (2023). doi:10.21012/FC11.092350.

[26] A. Baktheer, E. Martínez-Pañeda, F. Aldakheel, Phase field cohesive zone modeling for fatigue crack propagation in quasi-brittle materials, Computer Methods in Applied Mechanics and Engineering 422 (2024) 116834. doi:10.1016/j.cma.2024.116834.